

Study of Non-Standard Charged-Current Interactions at the MOMENT experiment

Jian Tang* and Yibing Zhang†

School of Physics, Sun Yat-Sen University, 510275, Guangzhou, China

(Dated: November 26, 2022)

MuOn-decay MEduM baseline NeuTrino beam experiment (MOMENT) is a next-generation accelerator neutrino experiment looking for more physics study. We try to simulate neutrino oscillations confronting with Charged-Current&Non-Standard neutrino Interactions(CC-NSIs) at MOMENT. These NSIs could alter neutrino production and detection processes and get involved in neutrino oscillation channels. We separate a perturbative discussion of oscillation channels at near and far detectors, and analyze parameter correlations with the impact of CC-NSIs. Taking δ_{cp} and θ_{23} as an example, we find that CC-NSIs can induce bias in precision measurements of standard oscillation parameters. In addition, a combination of near and far detectors using Gd-doped water cherenkov technology at MOMENT is able to provide good constraints of CC-NSIs happening at the neutrino production and detection processes.

PACS numbers: 13.15.+g, 14.60.Pq, 14.60.St

arXiv:1705.09500v1 [hep-ph] 26 May 2017

* tangjian5@mail.sysu.edu.cn

† zhangyb27@mail2.sysu.edu.cn

I. INTRODUCTION

In the past decades, we have seen enormous progress from neutrino oscillation experiments using solar, atmospheric, accelerator and reactor neutrinos [1–8]. In the framework of three neutrino oscillations, there are six physics parameters including three mixing angles θ_{12} , θ_{13} , θ_{23} , one Dirac CP phase δ_{cp} and two mass squared splittings Δm_{31}^2 , Δm_{21}^2 . According to a global analysis of these neutrino oscillation experiments [9–12], mixing angles θ_{12} , θ_{13} & θ_{23} and mass square differences Δm_{21}^2 & $|\Delta m_{31}^2|$ have been well measured so far. The mixing angle θ_{23} , however, has not been determined with enough precision to disentangle whether the mixing angle θ_{23} is 45° , while many discrete models point to a maximal mixing $\theta_{23} = 45^\circ$ with regard to a $\mu - \tau$ symmetry. In addition, a deviation from $\theta_{23} = 45^\circ$ causes an octant degeneracy problem in certain neutrino oscillation channels [13, 14]. Nonetheless, the Dirac CP phase describing the difference between matter and anti-matter as well as the sign of Δm_{31}^2 (normal mass hierarchy: $\Delta m_{31}^2 > 0$; inverted mass hierarchy: $\Delta m_{31}^2 < 0$) have not been well constrained yet. Despite recent results from T2K [15] and NO ν A [16] disfavors the inverted mass hierarchy at a low confidence level and give hints of $\delta_{CP} \approx -90^\circ$, we expect more data to draw a solid conclusion or further call for the next-generation experiments such as accelerator neutrino oscillation experiments like DUNE [17] and T2HK [18], the medium-baseline reactor experiments like JUNO [19] and RENO-50 [20], atmospheric neutrino experiments like INO [21], PINGU [22] and KM3Net [23].

New physics beyond Standard Model (SM) is around the corner which might offer the sub-leading non-standard neutrino interactions (NSIs) in nature, such as seesaw models, supersymmetry models, extra-dimension models and the like. Several studies have been conducted on NSIs from the experimental and model-building point of view [24–41]. A review of NSIs is given in detail in Ref. [42, 43]. With the help of an effective field theory, we can generally integrate out the mediator/propagator in the Feynman diagram and keep four fermions contact with each other. New physics scale is then embedded into the effective coupling constant $\epsilon_{\alpha'\beta'}^{\alpha\beta}$, where α/β or α'/β' are the related fermion flavours. In theory the higher the new physics scale, it is harder to reach the smaller effective coupling constant. We have reached the era of precision measurements of neutrino mixing parameters after an establishment of neutrino oscillation. It is promising for us to develop better neutrino detectors to search for sub-leading NSIs in the current and next-generation neutrino oscillation experiments as a complementary to the new physics search with the high intensity machine at the collider.

The MuOn-decay MEdium baseline NeuTrino beam experiment (MOMENT) is a next-generation accelerator neutrino experiment proposed for discovery of leptonic CP violation [44]. The atmospheric neutrino flux is a serious hindrance to the study of CP violation at MOMENT. The atmospheric neutrino background exceeds the oscillation signal events significantly at O(100) MeV. Neutrino beams from such a continuous proton accelerator provide high luminosity fluxes but result in a pathetic loss of timing information which is traditionally used to suppress atmospheric neutrino backgrounds in the accelerator neutrino oscillation experiment with the pulsed proton beam facility. A new detector technology, however, might overcome the barrier and offer precision tests of θ_{23} . The new detection technology might also lead to a discovery of the CP violating phase in the framework of 3-flavour neutrino oscillations [45], which complement the study at T2K and NO ν A to solve the degeneracy problem and exclude CP conserved phase at a relatively high confidence level. In addition, a comprehensive study of the bounds on NSI parameters has been carried out [46]. The bounds on NSI parameters governing the neutrino productions and detections are about one order of magnitude stronger than those related to neutrino propagation in matter, taking the current bounds on ϵ^{ud} and $\epsilon^{\mu e}$ as an example:

$$|\epsilon^{\mu e}| < \begin{pmatrix} 0.025 & 0.03 & 0.03 \\ 0.025 & 0.03 & 0.03 \\ 0.025 & 0.03 & 0.03 \end{pmatrix} \quad 90\% \text{C.L} \quad (1)$$

$$|\epsilon^{ud}| < \begin{pmatrix} 0.041 & 0.025 & 0.041 \\ 0.026 & 0.078 & 0.013 \\ 0.12 & 0.013 & 0.13 \end{pmatrix} \quad 90\% \text{C.L} \quad (2)$$

The perturbative discussions of the neutrino oscillation probabilities in the presence of source/detector and matter NSIs can be found in the reference [47], which is motivating further study and optimization of new experimental proposals to pin down the current bounds. The first glimpse of NSI effects during neutrino propagation in matter at MOMENT has been shown in the reference [48]. It has discussed the sensitivity of neutral-current NSIs by means of accelerator neutrino oscillations in matter. However, the impact of source and detector NSIs associated with charged-current interactions has not been discussed. Within a theoretical model predicting new neutrino interactions, it is natural and fair for neutrinos to carry new charged-current and neutral-current interactions during the production

process, the propagation process and the detection process. On the other hand, the current neutrino experiment T2K and NO ν A are based on the superbeam neutrino production where neutrinos come from pion decays. We have to stress that NSIs associated with muon decays are very different from those happening at pion decays if we take the new physics into account. Therefore, it is demanding to bring source/detector NSIs for a complete analysis at MOMENT where neutrinos are produced by muon decays.

In this work, we explore the charged current NSIs effects at MOMENT. We focus on the precision measurement of standard neutrino mixing parameters and constraints of NSI parameters in the presence of non-standard charged-current interactions at the source and detector. The paper is organized as follows: we discuss neutrino oscillation channels at a short and far distance in Section II. In Section III, we describe our implementations of MOMENT and simulation details. In Section IV, we show the impacts of NSIs on precision measurements of standard neutrino parameters and present the correlations and constraints of NSI parameters within production and detection at MOMENT, and compare the expected results with current bounds. The summary follows in Section V.

II. DISCUSSION OF NEUTRINO OSCILLATION CHANNELS

The formalism of NSI is a general way of studying the impacts of new physics in neutrino oscillations. Without dealing with the matter NSIs due to the short baseline, we start with the neutrino production and detection processes involving non-standard interactions. These processes are often related to the charged lepton and called the charged-current-like NSI. The neutrinos at the MOMENT experiment are produced by the muon decay processes $\mu^- \rightarrow e^- + \bar{\nu}_e + \nu_\mu$ and $\mu^+ \rightarrow e^+ + \nu_e + \bar{\nu}_\mu$ and are detected mainly through quasielastic charged-current interactions: $\nu_\ell + n \rightarrow p + \ell^-$ and $\bar{\nu}_\ell + p \rightarrow n + \ell^+$ (Here ℓ denotes e or μ) in the neutrino detector. The NSIs involved in the muon decay production process are related to charged leptons, while the NSIs involved in the detection process are associated with quarks. The muon decay together with CC-NSIs can be described by the effective Lagrangian density

$$\mathcal{L}_{NSI}^l = -2\sqrt{2}G_F \varepsilon_{\gamma\delta}^{\alpha\beta P} [\bar{\ell}_\alpha \gamma^\mu P \ell_\beta] [\bar{\nu}_\gamma \gamma_\mu P_L \nu_\delta] \quad (3)$$

Where P can be P_L or P_R determined by Hermiticity. For the muon decay, $\alpha = \mu$ and $\beta = e$. On the other hand, the quasielastic charged-current interactions with CC-NSIs are governed by the effective Lagrange density

$$\mathcal{L}_{NSI}^q = -2\sqrt{2}G_F \varepsilon_{\alpha\beta}^{qq'P} V_{qq'} [\bar{q} \gamma^\mu P q'] [\bar{\ell}_\alpha \gamma_\mu P_L \nu_\beta] + h.c. \quad (4)$$

For neutrino oscillation experiments, q represents up quark and q' represents down quark.

In the presence of the CC-NSIs, a neutrino source can not only produce a pure flavour neutrino eigenstate $|\nu_\alpha\rangle$, but rather a state with a mixture of different flavours:

$$|\nu_\alpha^s\rangle = |\nu_\alpha\rangle + \sum_{\beta=e,\mu,\tau} \epsilon_{\alpha\beta}^s |\nu_\beta\rangle \quad (5)$$

Similarly, the detector projects the neutrino wave function not only onto the standard weak eigenstates, but onto a combination of them:

$$\langle \nu_\beta^d | = \langle \nu_\beta | + \sum_{\alpha=e,\mu,\tau} \epsilon_{\alpha\beta}^d \langle \nu_\alpha | \quad (6)$$

Here $\epsilon_{\alpha\beta}^s$ and $\epsilon_{\alpha\beta}^d$ are defined via $\epsilon_{\alpha\beta}^{e\mu}$ and $\epsilon_{\alpha\beta}^{u\bar{d}}$, respectively. Thus the oscillation probability is

$$\begin{aligned} P(\nu_\alpha^s \rightarrow \nu_\beta^d) &= |\langle \nu_\beta^d | e^{-i\mathcal{H}L} | \nu_\alpha^s \rangle|^2 \\ &= |(1 + \epsilon^d)_{\gamma\beta} (e^{-i\mathcal{H}L})_{\gamma\delta} (1 + \epsilon^s)_{\alpha\delta}|^2 \\ &= |[(1 + \epsilon^d)^T e^{-i\mathcal{H}L} (1 + \epsilon^s)^T]_{\beta\alpha}|^2 \end{aligned} \quad (7)$$

The ϵ^s and ϵ^d are the charged-current NSI matrices for the production and detection, respectively. There are 18 NSI real parameters in each matrix, since the element $\epsilon_{\alpha\beta}^{s/d}$ consists of the amplitude $|\epsilon_{\alpha\beta}^{s/d}|$ and the phase $\phi_{\alpha\beta}^{s/d}$.

Since MOMENT is a medium baseline experiment, the matter effects are relatively small. We have checked the numerical results of oscillation probabilities in vacuum and matter, and found negligible difference with/without matter effects. This is also one of our motivations to focus on CC-NSIs. In the following sections, we will only, for sake of simplicity, display the probabilities in vacuum for related appearance and disappearance channels and try to extract useful information via the event rates. Of course, matter effects are taken into account simultaneously in the full simulation for physics performance study. Since near and far detectors will be used in the simulation later, we will discuss the oscillation channels at a short and far distance separately.

A. Oscillation channels at a near detector

Here a near detector means detecting neutrinos at a distance of $O(100)$ meters. In the standard oscillation frame without non-standard interactions, $\nu_\mu(\bar{\nu}_\mu)$ and $\nu_e(\bar{\nu}_e)$ can not develop neutrino oscillation patterns in such a short distance and their probabilities are equal to 1. However, NSIs are able to generate **zero-distance effects** so that the disappearance probabilities are allowed to be larger than 1, equal to 1, or smaller than 1. After dropping the terms $O(\epsilon^2)$, we approximate the probabilities as Eq. (8) and Eq. (9):

$$P_{\bar{\nu}_e^s \rightarrow \bar{\nu}_e^d}^{ND} \approx 1 + 2|\epsilon_{ee}^s| \cos \phi_{ee}^s + 2|\epsilon_{ee}^d| \cos \phi_{ee}^d \quad (8)$$

$$P_{\bar{\nu}_\mu^s \rightarrow \bar{\nu}_\mu^d}^{ND} \approx 1 + 2|\epsilon_{\mu\mu}^s| \cos \phi_{\mu\mu}^s + 2|\epsilon_{\mu\mu}^d| \cos \phi_{\mu\mu}^d \quad (9)$$

It is easy to see that $P(\bar{\nu}_e^s \rightarrow \bar{\nu}_e^d)/P(\bar{\nu}_\mu^s \rightarrow \bar{\nu}_\mu^d)$ deviates from unity with some constant terms in the presence of relevant NSI parameters ϵ_{ee}^s and ϵ_{ee}^d ($\epsilon_{\mu\mu}^s$ and $\epsilon_{\mu\mu}^d$). If neutrinos are produced with charged lepton decays and detected by identifying the same charged leptons, the contribution of ϵ_{ee}^s to the probability is equivalent to ϵ_{ee}^d and then the sensitivity to these two parameters should be the same at the near detector.

Similarly, the appearance channels $\nu_\mu \rightarrow \nu_e$ ($\nu_e \rightarrow \nu_\mu$) must remain zero in the standard 3-flavor neutrino scenario. After dropping the $O(\epsilon^3)$ and $O(\epsilon^4)$ terms, the expressions for ν_e and ν_μ appearance probabilities can be written as Eq. (10) and Eq. (11), respectively:

$$P_{\nu_\mu^s \rightarrow \nu_e^d}^{ND} \approx |\epsilon_{\mu e}^s|^2 + |\epsilon_{\mu e}^d|^2 + 2|\epsilon_{\mu e}^s||\epsilon_{\mu e}^d| \cos(\phi_{\mu e}^s - \phi_{\mu e}^d) \quad (10)$$

$$P_{\nu_e^s \rightarrow \nu_\mu^d}^{ND} \approx |\epsilon_{e\mu}^s|^2 + |\epsilon_{e\mu}^d|^2 + 2|\epsilon_{e\mu}^s||\epsilon_{e\mu}^d| \cos(\phi_{e\mu}^s - \phi_{e\mu}^d) \quad (11)$$

Here the $\nu_e(\nu_\mu)$ appearance probability would depend on $\epsilon_{\mu e}^s$ and $\epsilon_{\mu e}^d$ ($\epsilon_{e\mu}^s$ and $\epsilon_{e\mu}^d$) after we introduce the NSIs at the neutrino source and detector. It is a discovery of new physics to observe zero-distance effects at near detectors for disappearance or appearance channels. Compared with superbeam experiments, neutrinos produced by muon decays are purer and have a better chance for New Physics beyond Standard Model.

B. Oscillation channels at a far detector

In this section we display the probabilities in channels suitable for the far detector at MOMENT. In the standard framework describing three neutrino mixings, the probability of $\nu_\mu \rightarrow \nu_e$ channel is calculated by a simple change of sign of the $\sin \delta$ term in a T-reversed channel of $\nu_e \rightarrow \nu_\mu$. Due to CC-NSIs, $\nu_\mu \rightarrow \nu_e$ and $\nu_e \rightarrow \nu_\mu$ probabilities are not so obvious any more. We derive the explicit expressions of their probabilities in vacuum perturbatively derived as given in Eq. (12) and Eq. (13).

$$\begin{aligned} P_{\nu_\mu \rightarrow \nu_e}^{vac} = & s_{2 \times 13}^2 s_{23}^2 \sin^2 \Delta_{31} \\ & + \alpha \Delta_{31} s_{2 \times 12} s_{2 \times 23} s_{13} [\sin(2\Delta_{31}) \cos \delta - 2 \sin \delta \sin^2 \Delta_{31}] \\ & + \alpha^2 \Delta_{31}^2 c_{23}^2 s_{2 \times 12}^2 \\ & - |\epsilon_{\mu e}^s| s_{2 \times 13} s_{23} \sin(\delta + \phi_{\mu e}^s) \sin(2\Delta_{31}) \\ & - 2|\epsilon_{\mu e}^s| s_{2 \times 13} s_{23} \cos(\delta + \phi_{\mu e}^s) \sin^2 \Delta_{31} \\ & - |\epsilon_{\mu e}^d| s_{2 \times 13} s_{23} \sin(\delta + \phi_{\mu e}^d) \sin(2\Delta_{31}) \\ & - 2|\epsilon_{\mu e}^d| s_{2 \times 13} s_{23} c_{2 \times 23} \cos(\delta + \phi_{\mu e}^d) \sin^2 \Delta_{31} \\ & + 4|\epsilon_{\tau e}^d| c_{23} s_{2 \times 13} s_{23}^2 \cos(\delta + \phi_{\tau e}^d) \sin^2 \Delta_{31} \\ & - 2\alpha \Delta_{31} |\epsilon_{\mu e}^s| c_{13} s_{2 \times 12} c_{23} \sin \phi_{\mu e}^s \\ & + 2\alpha \Delta_{31} |\epsilon_{\mu e}^d| s_{2 \times 12} c_{13} c_{23} s_{23}^2 \cos \phi_{\mu e}^d \sin(2\Delta_{31}) \\ & - 2\alpha \Delta_{31} |\epsilon_{\mu e}^d| s_{2 \times 12} c_{13} c_{23} \sin \phi_{\mu e}^d (1 - 2s_{23}^2 \sin^2 \Delta_{31}) \\ & + 4\alpha \Delta_{31} |\epsilon_{\tau e}^d| c_{13} c_{23}^2 s_{2 \times 12} s_{23} \sin \phi_{\tau e}^d \sin^2 \Delta_{31} \\ & + 2\alpha \Delta_{31} |\epsilon_{\tau e}^d| c_{13} c_{23}^2 s_{2 \times 12} s_{23} \cos \phi_{\tau e}^d \sin(2\Delta_{31}) \\ & + O(\alpha^3) + O(\alpha^2 s_{13}) + O(\alpha s_{13}^2) + O(s_{13}^3) \\ & + O(\epsilon \alpha^2) + O(\epsilon s_{13}^2) + O(\epsilon^2) \end{aligned} \quad (12)$$

$$\begin{aligned}
P_{\nu_e \rightarrow \nu_\mu}^{vac} = & s_{2 \times 13}^2 s_{23}^2 \sin^2 \Delta_{31} \\
& + \alpha \Delta_{31} s_{2 \times 12} s_{2 \times 23} s_{13} [\sin(2\Delta_{31}) \cos \delta + 2 \sin \delta \sin^2 \Delta_{31}] \\
& + \alpha^2 \Delta_{31}^2 c_{23}^2 s_{2 \times 12}^2 \\
& + |\epsilon_{e\mu}^s| s_{2 \times 13} s_{23} \sin(\delta - \phi_{e\mu}^s) \sin(2\Delta_{31}) \\
& - 4 |\epsilon_{e\mu}^s| s_{2 \times 13} s_{23} c_{2 \times 23} \cos(\delta - \phi_{e\mu}^s) \sin^2 \Delta_{31} \\
& + 4 |\epsilon_{e\tau}^s| c_{23} s_{2 \times 13} s_{23}^2 \cos(\delta - \phi_{e\tau}^s) \sin^2 \Delta_{31} \\
& + |\epsilon_{e\mu}^d| s_{2 \times 13} s_{23} \sin(\delta - \phi_{e\mu}^d) \sin(2\Delta_{31}) \\
& - 2 |\epsilon_{e\mu}^d| s_{2 \times 13} s_{23} \cos(\delta - \phi_{e\mu}^d) \sin^2 \Delta_{31} \\
& + 2\alpha \Delta_{31} |\epsilon_{e\mu}^s| s_{2 \times 12} c_{13} c_{23} s_{23}^2 \cos \phi_{e\mu}^s \sin(2\Delta_{31}) \\
& - 2\alpha \Delta_{31} |\epsilon_{e\mu}^s| s_{2 \times 12} c_{13} c_{23} \sin \phi_{e\mu}^s (1 - 2s_{23}^2 \sin^2 \Delta_{31}) \\
& + 2\alpha \Delta_{31} |\epsilon_{e\tau}^s| c_{13} c_{23}^2 s_{2 \times 12} s_{23} \cos \phi_{e\tau}^s \sin(2\Delta_{31}) \\
& + 4\alpha \Delta_{31} |\epsilon_{e\tau}^s| c_{13} c_{23}^2 s_{2 \times 12} s_{23} \sin \phi_{e\tau}^s \sin^2 \Delta_{31} \\
& - 2\alpha \Delta_{31} |\epsilon_{e\mu}^d| c_{13} s_{2 \times 12} c_{23} \sin(\phi_{e\mu}^d) \\
& + O(\alpha^3) + O(\alpha^2 s_{13}) + O(\alpha s_{13}^2) + O(s_{13}^3) \\
& + O(\epsilon \alpha^2) + O(\epsilon s_{13}^2) + O(\epsilon^2)
\end{aligned} \tag{13}$$

which are important channels to measure the CP-violating phase δ and octant of θ_{23} . Here $s_{ij} = \sin \theta_{ij}$, $c_{ij} = \cos \theta_{ij}$, $s_{2 \times ij} = \sin 2\theta_{ij}$, $c_{2 \times ij} = \cos 2\theta_{ij}$, $\Delta_{31} = \frac{\Delta m_{31}^2 L}{4E}$, $\alpha = \frac{\Delta m_{21}^2}{\Delta m_{31}^2}$ and $\epsilon_{\alpha\beta}^{s/d} = |\epsilon_{\alpha\beta}^{s/d}| e^{i\phi_{\alpha\beta}^{s/d}}$.

Similar to the discussion above, ν_μ and ν_e disappearance channel probabilities are given as Eq. (14) and Eq. (15) :

$$\begin{aligned}
P_{\nu_\mu^s \rightarrow \nu_\mu^d}^{vac} \approx & 1 - s_{2 \times 23}^2 \sin^2 \Delta_{31} \\
& + 2 |\epsilon_{\mu\mu}^s| \cos \phi_{\mu\mu}^s + 2 |\epsilon_{\mu\mu}^d| \cos \phi_{\mu\mu}^d \\
& - [2 |\epsilon_{\mu\mu}^s| \cos \phi_{\mu\mu}^s + 2 |\epsilon_{\mu\mu}^d| \cos \phi_{\mu\mu}^d] s_{2 \times 23}^2 \sin^2 \Delta_{31} \\
& - 2 (|\epsilon_{\mu\tau}^s| \cos \phi_{\mu\tau}^s + |\epsilon_{\tau\mu}^d| \cos \phi_{\tau\mu}^d) c_{2 \times 23} s_{2 \times 23} \sin^2 \Delta_{31} \\
& + (|\epsilon_{\mu\tau}^s| \sin \phi_{\mu\tau}^s + |\epsilon_{\tau\mu}^d| \sin \phi_{\tau\mu}^d) s_{2 \times 23} \sin(2\Delta_{31})
\end{aligned} \tag{14}$$

$$\begin{aligned}
P_{\nu_e^s \rightarrow \nu_e^d}^{vac} \approx & 1 - 4s_{13}^2 \sin^2 \Delta_{31} \\
& + 2 |\epsilon_{ee}^s| \cos \phi_{ee}^s + 2 |\epsilon_{ee}^d| \cos \phi_{ee}^d \\
& - 4 |\epsilon_{e\mu}^s| s_{13} s_{23} \cos(\delta - \phi_{e\mu}^s) \sin^2 \Delta_{31} \\
& + 2 |\epsilon_{e\mu}^s| s_{13} s_{23} \sin(\delta - \phi_{e\mu}^s) \sin(2\Delta_{31}) \\
& - 4 |\epsilon_{e\tau}^s| s_{13} c_{23} \cos(\delta - \phi_{e\tau}^s) \sin^2 \Delta_{31} \\
& + 2 |\epsilon_{e\tau}^s| s_{13} c_{23} \sin(\delta - \phi_{e\tau}^s) \sin(2\Delta_{31}) \\
& - 4 |\epsilon_{\mu e}^d| s_{13} s_{23} \cos(\delta + \phi_{\mu e}^d) \sin^2 \Delta_{31} \\
& - 2 |\epsilon_{\mu e}^d| s_{13} s_{23} \sin(\delta + \phi_{\mu e}^d) \sin(2\Delta_{31}) \\
& - 4 |\epsilon_{\tau e}^d| s_{13} c_{23} \cos(\delta + \phi_{\tau e}^d) \sin^2 \Delta_{31} \\
& - 2 |\epsilon_{\tau e}^d| s_{13} c_{23} \sin(\delta + \phi_{\tau e}^d) \sin(2\Delta_{31})
\end{aligned} \tag{15}$$

From the ν_μ (ν_e) disappearance channel the sensitivities to the parameter $|\epsilon_{ee}^s|$ and ϵ_{ee}^d ($\epsilon_{\mu\mu}^s$ and $\epsilon_{\mu\mu}^d$) are expected to be observed. The $\nu_\mu \rightarrow \nu_\mu$ is an important channel to measure θ_{23} , which is expected to judge whether θ_{23} is maximal or not.

We immediately read the impacts of NSI parameters on each channel in order:

- It is clear that $\nu_\mu \rightarrow \nu_e$ is affected by the dominant NSI parameters $\epsilon_{\mu e}^s$, $\epsilon_{\mu e}^d$ and $\epsilon_{\tau e}^d$. If we do not consider those terms involving the CP phases from NSIs, turning on $\epsilon_{\mu e}^s$ and $\epsilon_{\tau e}^d$ is approximately equivalent to enlarging or compressing the amplitude of $\sin^2 \Delta_{31}$, while the $\epsilon_{\mu e}^d$ will change the maximal amplitude of its oscillation probability.
- Similarly, $\nu_e \rightarrow \nu_\mu$ channel is mainly determined by $\epsilon_{e\mu}^s$, $\epsilon_{e\tau}^s$ and $\epsilon_{e\mu}^d$, apart from standard neutrino mixing parameters. $\epsilon_{e\tau}^s$ and $\epsilon_{e\mu}^d$ change the amplitude of $\sin^2 \Delta_{31}$ and $\epsilon_{e\mu}^s$ shifts the location of the peak at the neutrino oscillation probability curve.

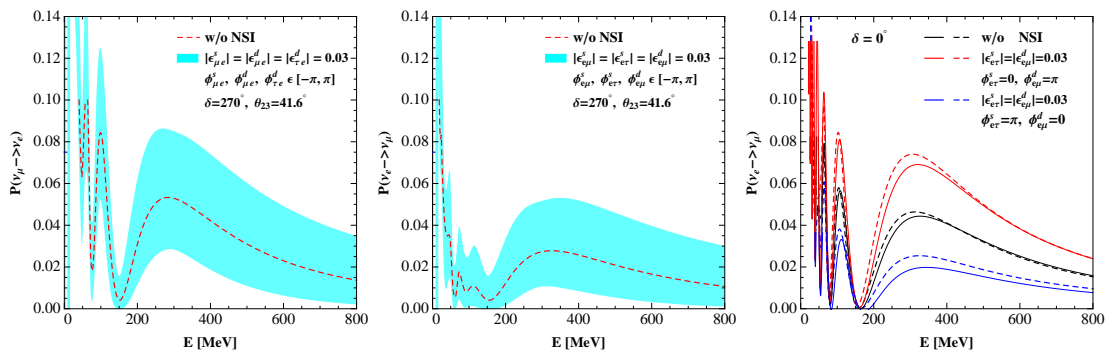


FIG. 1. The oscillation probabilities of $P(\nu_\mu \rightarrow \nu_e)$ and $P(\nu_e \rightarrow \nu_\mu)$ with/without CC-NSIs at a far detector given the baseline of 150 km. In the left and central panels, the shaded region in cyan is due to the variation of relevant NSI parameters as is shown in the legend. The dashed red line represents the case without NSI parameters. In the right panel, probabilities for $P(\nu_e \rightarrow \nu_\mu)$ are compared between a perturbative approximation given by continuous lines exact numerical calculation shown by the dashed lines. The standard mixing parameters by default follow the global fits.

- Since these NSI parameters are entangled with θ_{23} and CP-violating phase δ , NSIs would interfere with precision measurements of the standard CP-violating phase δ and θ_{23} which is manifested by related terms in Eq. (12) and Eq. (13).

In Fig. 1, we make a comparison of the probabilities of $P(\nu_\mu \rightarrow \nu_e)$ and $P(\nu_e \rightarrow \nu_\mu)$ with/without NSIs. We turn on non-vanishing parameters of $|\epsilon_{\mu e}^s| = |\epsilon_{\mu e}^d| = |\epsilon_{\tau e}^d| = 0.03$ for an illustration. The amplitude of oscillation pattern is shifted significantly by these NSI impacts as we point out from the perturbative approximation. Firstly, the left and central panels display the standard three flavour probability curves and the probability bands originating from the variations of NSI parameters. The shaded region in the left and central panels of Fig. 1 shows changes of oscillation probabilities when the standard CP-violating phase is $3\pi/2$ and the NSI phases vary in $[-\pi, \pi]$. It is easy to see the difference of $P(\nu_\mu \rightarrow \nu_e)$ and $P(\nu_e \rightarrow \nu_\mu)$ assuming all NSI parameters are turned off, where $P(\nu_\mu \rightarrow \nu_e) - P(\nu_e \rightarrow \nu_\mu)$ becomes negative for $\delta \in (0, \pi)$ and $P(\nu_\mu \rightarrow \nu_e)$ is larger than $P(\nu_e \rightarrow \nu_\mu)$ for $\delta \in (\pi, 2\pi)$; with $\delta = 0/\pi$, there is no difference between $P(\nu_\mu \rightarrow \nu_e)$ and $P(\nu_e \rightarrow \nu_\mu)$. However, once we turn on NSI parameters, the relationship between the probabilities of these two channels will be changed as can be seen from the shaded regions. We next in the right panel show the analytical and numerical calculations for probability $P(\nu_e \rightarrow \nu_\mu)$ with solid and dashed lines, respectively. The differences between two calculation approaches are due to the negligible terms in the analytical calculations. In addition, this panel indicates a correlation of new parameters such as $\epsilon_{e\tau}^s$ and $\epsilon_{e\mu}^d$. In the right panel of Fig. 1, we cross check the perturbative approximation given by continuous lines exact numerical calculation shown by the dashed lines. They are matching very well, though there is a small discrepancy due to a loss of the higher-order terms in the perturbation. After we introduce the characteristics of MOMENT and simulation details in the next section, we will be further convinced with analysis of event rates for the correlation between $\epsilon_{\mu e}^s$ and $\epsilon_{\mu e}^d$ as shown in Fig. 2.

III. CHARACTERISTICS OF MOMENT AND SIMULATION DETAILS

Continuous high-energy proton beam at 1.5 GeV with a power of 15 MW will be produced in the accelerator facility. A choice of target stations with mercury is still under optimization to generate charged mesons most of which are pions and kaons. We can expect 1.1×10^{24} Proton On Target (POT) per year. A magnetic solenoid will be deployed to make the pion beam focused and selected, and the curvature of solenoid helps selecting muons from pion decays followed by a straight tunnel to prepare neutrinos from muon decays. The neutrino fluxes are provided by the accelerator working group in MOMENT for our physics performance study [49]. We intend to extract more information from eight oscillation channels by the muon-decay neutrino beams in the simulation study: $\nu_e \rightarrow \nu_e$, $\nu_e \rightarrow \nu_\mu$, $\nu_\mu \rightarrow \nu_e$, $\nu_\mu \rightarrow \nu_\mu$ and their conjugate partners. Since we have to conduct flavour and charge identifications to distinguish secondary particles, we consider the new technology using Gd-doping water to separate both Cherenkov and coincident signals from capture of thermal neutrons. Muon taggings can be efficiently obtained by daughter electrons together with pulse shape discrimination of waveforms. We follow the detector description from a sophisticated study in the CERN-MEMPHYS project [50] and update the related new technology with regard to Gd-doping water. The major backgrounds for MOMENT come from atmospheric neutrinos. We believe that it can be suppressed by the beam direction and proper modelling background spectra within the beam-off period.

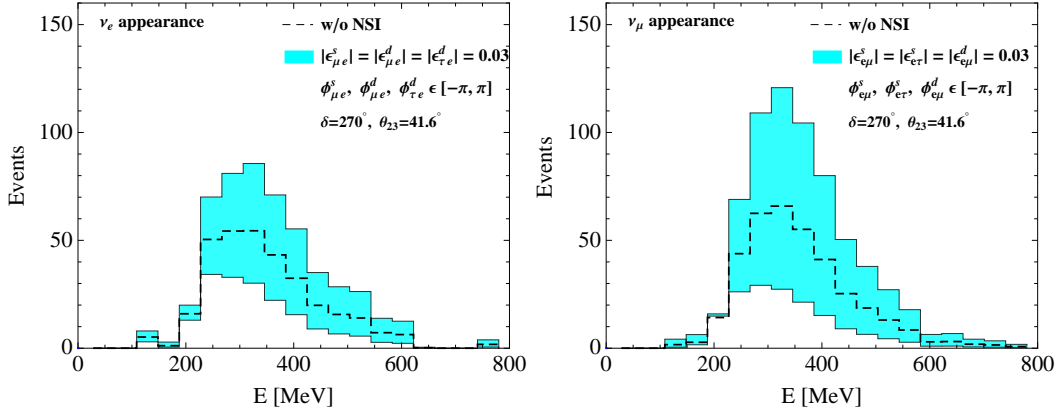


FIG. 2. The event rates of $\nu_\mu \rightarrow \nu_e$ and $\nu_e \rightarrow \nu_\mu$ channels versus the neutrino energy. Variations of the relevant NSI parameters give rise to the cyan bands. The dashed black lines represent the case without NSIs.

Parameters	Best-fit values	Prior uncertainties
$\theta_{12}/^\circ$	33.56	2.3%
$\theta_{13}/^\circ$	8.46	1.8%
$\theta_{23}/^\circ$	41.6	5.8%
$\Delta m_{21}^2/\text{eV}^2$	7.5×10^{-5}	2.4%
$\Delta m_{31}^2/\text{eV}^2$	2.524×10^{-3}	1.6%

TABLE I. The best-fit values of standard parameters and their prior uncertainties adopted in the numerical simulations [12].

The charged-current interactions are used to identify neutrino signals:

$$\begin{aligned}
 \nu_e + n &\rightarrow p + e^- & \bar{\nu}_\mu + p &\rightarrow n + \mu^+ \\
 \bar{\nu}_e + p &\rightarrow n + e^+ & \nu_\mu + n &\rightarrow p + \mu^-
 \end{aligned}$$

A few remarks for signals and backgrounds are given as follows:

- Gd doping into pure water could be used to discriminate electron neutrinos and antineutrinos by whether there is a capture of the scattered thermal neutron or not. Neutron capture on Gd emits the 8 MeV gamma rays. The $\bar{\nu}_e$ ($\bar{\nu}_\mu$) signal is reconstructed by tagging the neutron in coincidence with the positron to suppress most of backgrounds associated with single events. While the water Cherenkov detection is not significantly changed, ν_e signals come from the Cherenkov ring created by ν_e elastic scattering with electrons.
- In a Water Cherenkov detector, electron and muon-flavour neutrinos are well separated by event reconstructions, where the former type creates electron showers and the latter type leads to muon tracks. Sometimes, low-energy muons decay and cause flavour misidentifications. Here we ignore the flavour misidentification in the simulation.
- The imperfection of detectors leads to misidentifications of charge-current interactions for neutrino signals. Here we suppose their effects are negligible.
- It is also possible for neutral-current interactions with the accidental single events to be identified as the coincident signal. Neutron knocks a nucleus off an oxygen, resulting in excited states and photons from de-excitations will mimick $\bar{\nu}_e$ signals oscillated from accelerator neutrino beams. We expect them to be rather small and assign an extremely small background over signal ratio in our simulation.

Table II lists the simulation details about the neutrino detector. A baseline of 150 km is assigned in the current proposal [44] based on the neutrino beam energy range. For the detector fiducial masses and the running time for each polarity we follow Ref. [44, 45]. In the massive water cherenkov detector, we follow electron and muon selection efficiencies given in Ref. [51, 52]. The charged identification ratio for distinguishing the neutrinos from antineutrinos could be found in Ref. [52]. With regard to the normalization error on signals and the normalization error on backgrounds, we refer to Ref. [53]. As for the atmospheric backgrounds, it could be suppressed via sending

Fiducial mass (ND/FD)	Gd-doping Water cherenkov (100 t/500 kton)
Baseline (ND/FD)	500 m/150 km
Channels	$\nu_e(\bar{\nu}_e) \rightarrow \nu_e(\bar{\nu}_e), \nu_\mu(\bar{\nu}_\mu) \rightarrow \nu_\mu(\bar{\nu}_\mu)$ $\nu_e(\bar{\nu}_e) \rightarrow \nu_\mu(\bar{\nu}_\mu), \nu_\mu(\bar{\nu}_\mu) \rightarrow \nu_e(\bar{\nu}_e)$
Energy resolution	$8.5\%/\sqrt{E}$
Runtime	μ^- mode 5 yrs+ μ^+ mode 5 yrs
Energy range	100 MeV to 800 MeV
Efficiency	$\nu_\mu(\bar{\nu}_\mu)$ selection: 50% $\nu_e(\bar{\nu}_e)$ selection: 40%
Normalization error on signal	appearance channels: 2.5% disappearance channels: 5%
Normalization error on background	5% (all channels)
Background sources	flavour misidentification charge misidentification atmospheric neutrinos

TABLE II. Assumptions for near and far detectors in the simulation.

the neutrino beam in short bunches with a suppression factor of 2.2×10^{-3} [54]. We follow similar descriptions in a beta beam experiment as given in Ref. [50, 55]. The cross section for quasi-elastic interactions is taken from the reference [56].

The values of the standard neutrino oscillation parameters are taken from the latest nu-fit results [12]. Table I shows the central values and their uncertainties in the present work. Unless otherwise mentioned, we expect a determination of mass hierarchy before running MOMENT and assume the normal mass hierarchy in our simulation without a loss of generality, i.e. $\Delta m_{31}^2 > 0$. A list of assumptions for near and far detectors are given in Table II. We present numerical results by simulating the neutrino oscillation signals and backgrounds using GLOBES [57, 58]. Similar to the probability-level analysis given in Fig. 1, we present event rates of $\nu_\mu \rightarrow \nu_e$ and $\nu_e \rightarrow \nu_\mu$ channels versus the neutrino energy in Fig. 2. The event spectra are shifted significantly after we consider the CC-NSI effects. The shaded region highlights the large variation from the new CP phases caused by CC-NSIs even if we fix their strength of NSI couplings. It is then straightforward to discuss physics performance for the MOMENT experiment with simulated event spectra.

IV. PHYSICS PERFORMANCE OF MOMENT

A. Impacts on precision measurements of standard mixing parameters by CC-NSIs

The CKM mixing matrix is well measured in the quark sector at the sub-percent level [59], while mixing parameters in the lepton sector are far away from such a precision. It is very likely for the next-generation experiment like MOMENT to achieve the goal doing precision measurements. In this section, we take the Dirac CP-violating phase δ_{CP} and θ_{23} as an illustration to show the impacts from CC-NSIs. The true value of θ_{23} is taken as 41.6° . We choose two δ values with $\delta = \pi/2$ and $\delta = 3\pi/2$ to simulate all oscillation channels at MOMENT and fit the neutrino spectra with/without NSIs. Fig. 3 demonstrates the numerical results. The true values of the standard oscillation parameters are shown by a red point in each panel. In all sub-figures (a), (b) and (c), we have considered uncertainties of standard mixing parameters. Panels like (a1) and (a2) show the determination of δ_{CP} and θ_{23} in the case of the standard neutrino oscillation without NSIs. By running MOMENT, we can determine the mixing angle θ_{23} with an error bar of one degree at the 3σ confidence level, while the precision for δ_{CP} is good enough. In sub-figure (b) and (c), NSIs happening at the source and detector are turned on. All the corresponding CC-NSI phases can vary within $(0, 2\pi)$. In the panel (b1) and (b2), we only consider the CC-NSIs ($\epsilon_{e\mu}^s, \epsilon_{e\tau}^s$ and $\epsilon_{e\mu}^d$, and their marginalization ranges are allowed within the current bounds given in Eq. (1) and Eq. (2).) which are related to $\nu_\mu(\bar{\nu}_\mu)$ appearance channels. The panels (b1)& (b2) show the enlarged uncertainties in parameter fittings. Especially, a degeneracy pops up in the measurement of $\theta_{23}-\delta_{\text{CP}}$ for the case of $\delta = 3\pi/2$, while it is still safe for the case of $\delta = \pi/2$. Furthermore, we go to panels (c1)/(c2) by turning on those CC-NSIs related to the $\nu_e(\bar{\nu}_e)$ and $\nu_\mu(\bar{\nu}_\mu)$ appearance channels ($\epsilon_{e\mu}^s, \epsilon_{e\tau}^s, \epsilon_{e\mu}^d$,

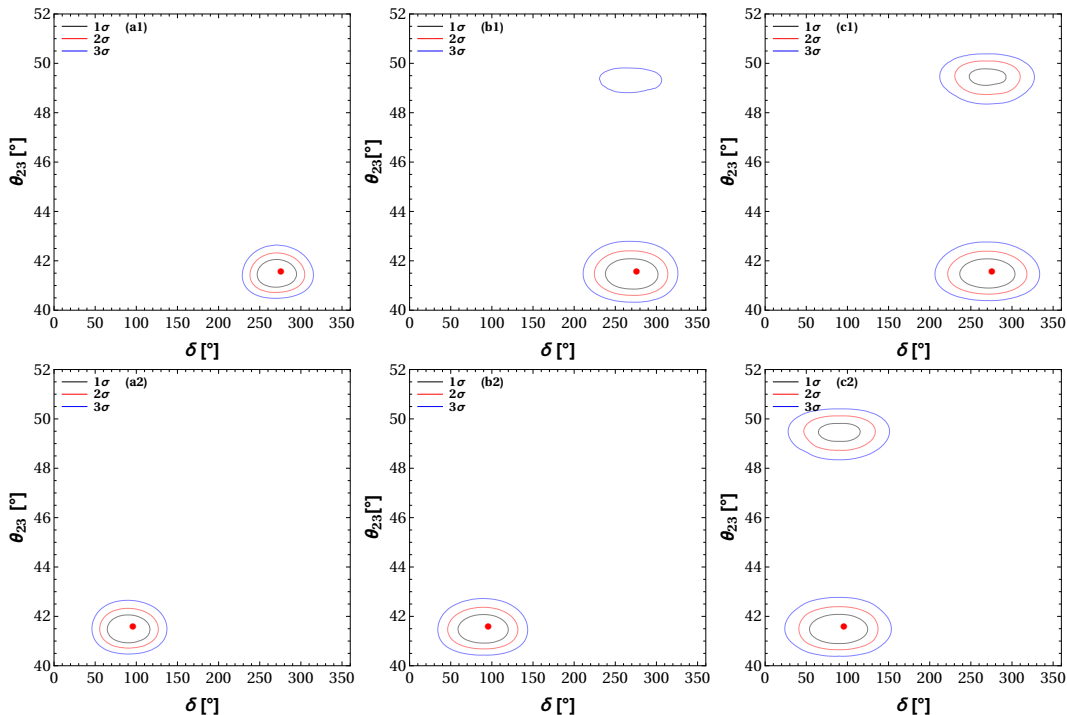


FIG. 3. The allowed region for $\theta_{23} - \delta$ for MOMENT. Panels (a) shows the determination of δ and θ_{23} in the case of the standard three flavour frame. In panel (b) we only consider the NSIs: $\epsilon_{e\mu}^s$, $\epsilon_{e\tau}^s$ and $\epsilon_{\tau e}^d$ which are related to ν_μ appearance channels. (c) shows the effects of those NSIs related to the ν_μ ($\bar{\nu}_\mu$) and ν_e (ν_e) appearance channels: $\epsilon_{e\mu}^s$, $\epsilon_{e\mu}^d$, $\epsilon_{e\tau}^s$, $\epsilon_{\mu e}^s$, $\epsilon_{\mu e}^d$, $\epsilon_{\tau e}^d$ and marginalization ranges are within current bounds given in Eq. (1) and Eq. (2). All of the corresponding phases can vary in $(0, 2\pi)$. The red points in all panels indicate the true values.

$\epsilon_{\mu e}^s$, $\epsilon_{\mu e}^d$, $\epsilon_{\tau e}^d$ and their marginalization ranges are within current bounds given in Eq. (1) and Eq. (2)).

As we have discussed in Section II, the ν_e appearance channel is affected by the parameters: $\epsilon_{\mu e}^s$, $\epsilon_{\mu e}^d$, $\epsilon_{\tau e}^d$, while the ν_μ appearance channel are mainly determined by the parameters $\epsilon_{e\mu}^s$, $\epsilon_{e\tau}^s$, and $\epsilon_{e\mu}^d$. This feature can be understood after a closer look at the Eq. (13). If δ is equal to $\pi/2$, the peak of the probability in $\nu_e \rightarrow \nu_\mu$ channel is much larger than the case of $\delta = 3\pi/2$. In turn, the number of event rates in the detector for $\delta = \pi/2$ are much higher. The corresponding fitted results are much better. Therefore, CC-NSI parameters destroy the precise determinations of standard mixing parameters. As can be seen from panels (c1) and (c2), the degeneracy even shows up at high confidence levels when we consider all the relevant NSI parameters. We might get into the wrong best-fit region if we neglect the CC-NSIs from the new physics. A combination of different neutrino oscillation experiments might resolve such an ambiguity and finish the task of precision measurements of neutrino mixing parameters to the same level as quark mixing parameters. Or we need the most powerful machine like a neutrino factory.

B. Correlations and constraints of NSI parameters

We have factorized the NSIs by integrating the potential heavy propagator from the new physics scale. Each NSI parameter has a magnitude which tells us the strength of new couplings and its associated phase to bridge the CP violating story. Therefore, it is convenient to adopt two methods: one is to take the NSI parameters as real, which corresponds to the strength of the coupling constant or switch off the NSI-induced CP violation phases; the other is to keep general assumptions given complex NSI parameters. In this section we discuss the constraints to source and detector NSIs from the far and near detector, respectively. For the former case, Table III demonstrates the sensitivity of MOMENT to constrain the NSI parameters using the single-parameter-fit at 90% C.L. The results are obtained by using all the neutrino and antineutrino oscillation channels with both near and far detectors. In a comparison of the current bounds and the expected limits from our simulation, we find that the MOMENT experiment with running time of 5+5 years has a good potential to improve the constraints for the CC NSIs. In this table, one can observe that most of the bounds for NSIs are improved except for $\epsilon_{e\tau}^s$, $\epsilon_{\mu\tau}^s$ and $\epsilon_{\tau e}^d$ which are marked by red fonts.

In the following part, we will focus on the exclusion curve to the amplitude versus its corresponding phase for each

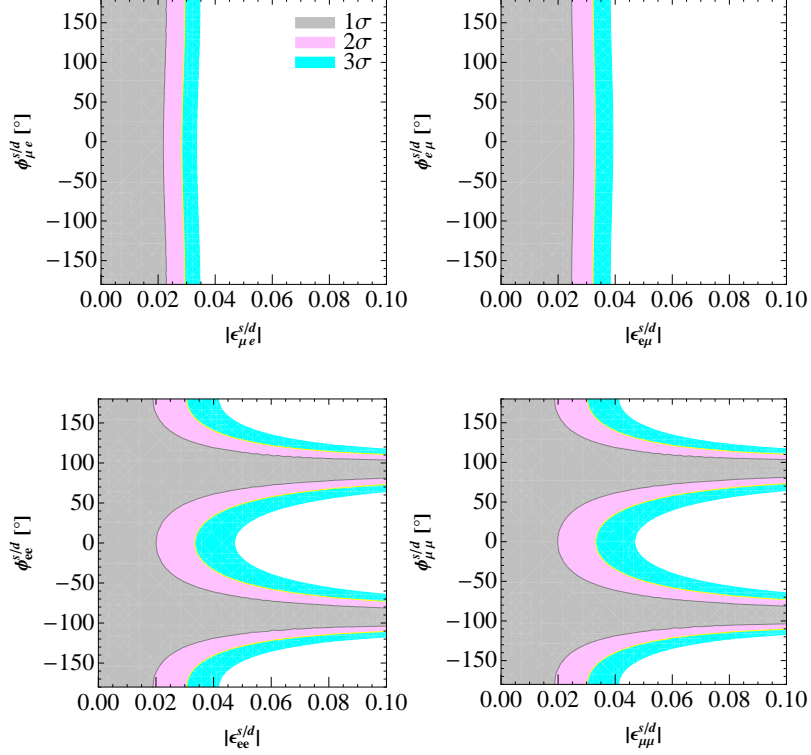


FIG. 4. Exclusion curves for the $|\epsilon_{\alpha\beta}^{s/d}| - \phi_{\alpha\beta}^{s/d}$ planes obtained by the near detector. The gray, magenta and cyan regions are the allowed regions at 1 σ , 2 σ and 3 σ C.L., respectively.

NSI parameter. Based on the previous discussions in Section. II, we neglect certain parameters which have trivial influence on the probabilities. At the near detector, we pay more attention to these parameters: $\epsilon_{ee}^{s/d}$, $\epsilon_{\mu\mu}^{s/d}$, $\epsilon_{\mu e}^{s/d}$ and $\epsilon_{e\mu}^{s/d}$. At the far detector, parameters $\epsilon_{ee}^s, \epsilon_{\mu\mu}^s, \epsilon_{\mu\tau}^s, \epsilon_{\mu e}^s, \epsilon_{\mu e}^d, \epsilon_{\tau e}^d, \epsilon_{e\mu}^s, \epsilon_{e\tau}^s$ and $\epsilon_{e\mu}^d$ are taken into account. The results at a near/far detector are presented in Fig. 4 and Fig. 5, respectively. We generate the event spectra with the true central values of standard oscillation parameters given in Table I. Then we turn on one NSI parameter and scan its amplitude and phase to fit the data. In Fig. 4, we show the excluded parameter space without any color at a near detector.

Parameter	ND constraints	FD constraints	ND+FD constraints	Current bounds
$ \epsilon_{ee}^s $	0.027	0.028	0.018	0.025
$ \epsilon_{e\mu}^s $	0.023	0.018	0.014	0.03
$ \epsilon_{e\tau}^s $	n/a	0.065	0.065	0.03
$ \epsilon_{\mu e}^s $	0.025	0.021	0.015	0.025
$ \epsilon_{\mu\mu}^s $	0.028	0.029	0.019	0.03
$ \epsilon_{\mu\tau}^s $	n/a	0.054	0.054	0.03
$ \epsilon_{ee}^d $	0.027	0.028	0.027	0.041
$ \epsilon_{e\mu}^d $	0.023	0.015	0.013	0.026
$ \epsilon_{\mu e}^d $	0.025	0.022	0.025	0.025
$ \epsilon_{\mu\mu}^d $	0.028	0.03	0.028	0.078
$ \epsilon_{\tau e}^d $	n/a	0.065	0.065	0.041
$ \epsilon_{\tau\mu}^d $	n/a	0.054	0.054	0.013

TABLE III. Expected 90% credible regions on NSI parameters with a single detector or a combination of near and far detectors at the MOMENT experiment. Here NSI parameters are assumed to be real, or NSI-induced CP phases are switched off.

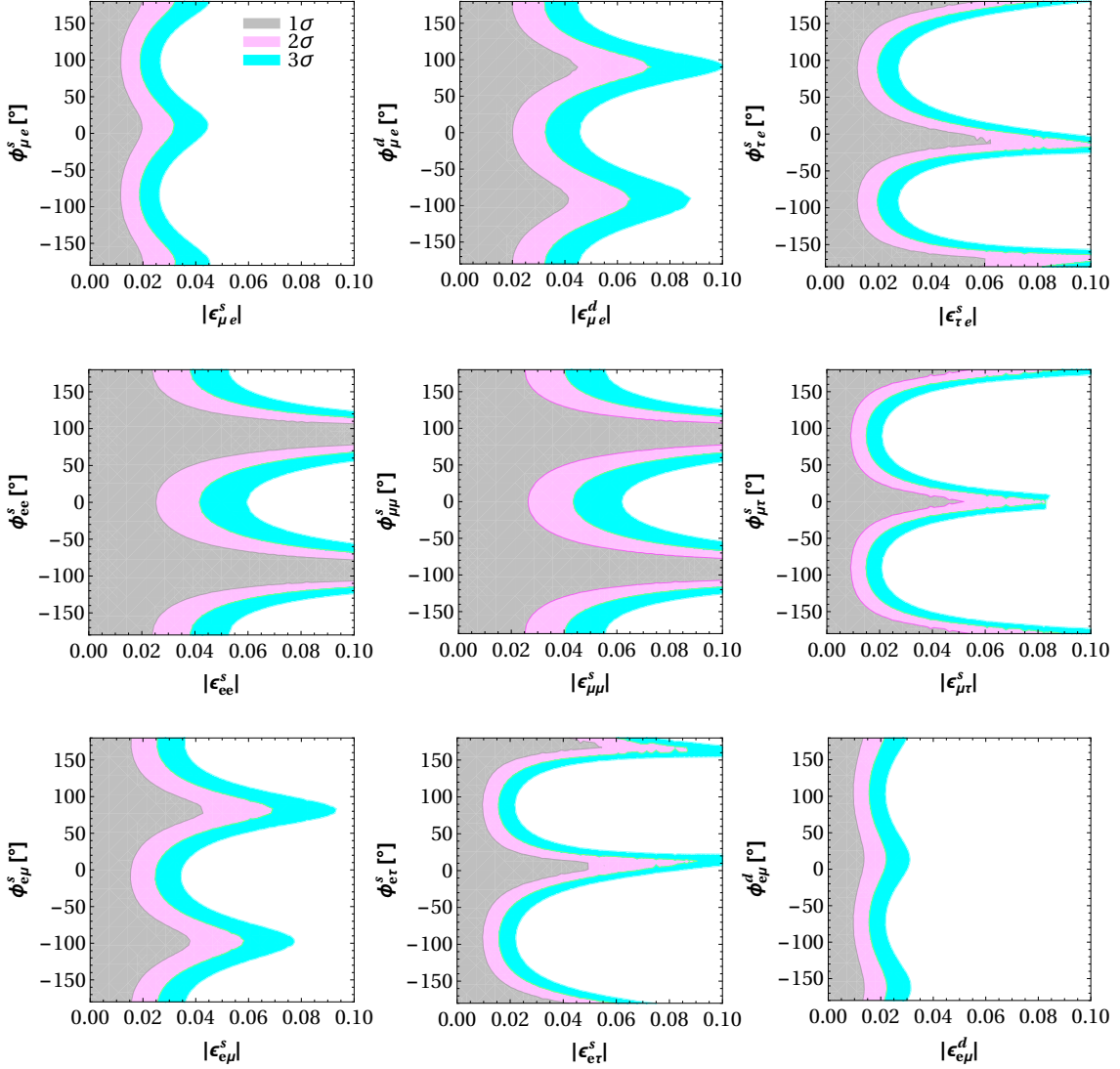


FIG. 5. Exclusion limits in the $|\epsilon_{\alpha\beta}^{s/d}| - \phi_{\alpha\beta}^{s/d}$ plane obtained from the far detector. The gray, magenta and cyan regions are the allowed regions at 1σ , 2σ and 3σ C.L., respectively.

One can observe that ν_μ disappearance channel almost has the same performance with the ν_e disappearance channel. When $\phi_{ee}^{s/d}$ ($\phi_{\mu\mu}^{s/d}$) equals to $\pm\pi$ or zero, the corresponding amplitude $|\epsilon_{ee}^{s/d}|$ ($|\epsilon_{\mu\mu}^{s/d}|$) has the best limit. When these phases are equal to $\pm\pi/2$, the sensitivity to the amplitude would disappear. For the ν_e (ν_μ) appearance channels, the constraint to $|\epsilon_{\mu e}^{s/d}|$ ($|\epsilon_{e\mu}^{s/d}|$) is almost irrelevant to the phase $\phi_{\mu e}^s$ ($\phi_{e\mu}^d$) supposing we only consider the source NSI parameter $\epsilon_{\mu e}^s$ or detector NSI parameter $\epsilon_{\mu e}^d$. This is because the term containing the phases $\phi_{\mu e}^s$ and $\phi_{\mu e}^d$ plays an important role in two amplitudes as can be seen from Eq. (10) and Eq. (11). Appearance channels can well constrain the magnitude of related CC-NSI parameters while they barely have impacts on their phases. On the other hand, disappearance channels exclude a large parameter space allowed in the current experimental bounds. There is a strong correlation between coupling strength and its phases in the neutrino oscillation experiment.

In Fig. 5, we switch to the sensitivities of CC-NSI parameters at a far detector. The colorful regions are allowed after we run a far detector at the MOMENT experiment. Here we list the features about the exclusion curves at the far detector for MOMENT:

- Since we can take advantage of the ν_e ($\bar{\nu}_e$) channel in MOMENT, obtaining the sensitivities of $\epsilon_{e\tau}^s$, $\epsilon_{e\mu}^s$ and $\epsilon_{e\mu}^d$ would be accessible. However, these parameters can not be observed well in superbeam experiments.
- The sensitivities to $\epsilon_{e\mu}^s$ and $\epsilon_{e\tau}^s$ are mainly extracted from the ν_e and ν_e appearance channels. It should be noted,

however, that the ν_e and $\bar{\nu}_e$ disappearance channels can help to enhance the constraints to these parameters. Similarly, with contributions from ν_e and $\bar{\nu}_e$ disappearance channels, the sensitivities to $\epsilon_{\mu e}^d$ and $\epsilon_{\tau e}^d$ which are mainly from ν_μ and $\bar{\nu}_\mu$ appearance channels will be improved.

- When the corresponding phases are around $\pm\pi/2$, the sensitivities to the amplitudes of ϵ_{ee}^s and $\epsilon_{\mu\mu}^s$ will vanish at the disappearance channels. However, the other NSI parameters do not have this problem.
- There are some symmetric relationships between the source and detector NSI parameters, such as the pair of $\epsilon_{\mu\tau}^s$ and $\epsilon_{\tau\mu}^d$, the pair of ϵ_{ee}^s and ϵ_{ee}^d , the pair of $\epsilon_{\mu\mu}^s$ and $\epsilon_{\mu\mu}^d$. It is not surprising at all, since the pair of effective coupling constants will be the same for neutrinos produced and detected by the same charged leptons.

The far detector has a good sensitivity of NSI parameters, especially for $\epsilon_{e\mu}^d$, $\epsilon_{e\tau}^s$ and $\epsilon_{\mu e}^s$. The numerical results about the correlations between the amplitudes and phases can again be interpreted with the previous probability formulas. Almost all NSI-induced phases change the exclusion limits severely except the e-mu sector. Meanwhile, limits on other sectors are not as good as those on the e-mu stamped CC-NSIs. Therefore, MOMENT using muon-decay beams has its unique capability of improving the constraints on $\epsilon_{e\mu}^d$ and $\epsilon_{\mu e}^s$.

V. SUMMARY AND CONCLUSIONS

New Physics beyond SM might cause non-standard neutrino interactions and leave imprints at the neutrino oscillation. The next-generation accelerator neutrino experiment MOMENT intends to produce the powerful neutrino beam with an energy of O(100) MeV by muon decays and leaves plenty of room for detector selections and physics study. At this energy range, quasi-elastic neutrino interactions dominate the detection process and backgrounds from π^0 are highly suppressed. Compared with traditional superbeams from charged meson decays where intrinsic backgrounds have to be alleviated by the off-axis technology like T2K and NO ν A, beams from muon decays are cleaner neutrino sources and good at a detection of new physics. CC-NSIs happening at neutrino productions and detections point to the new phenomenon, where a neutrino produced or detected together with the charged lepton will not necessarily share the same flavour, and flavour conversion is present already at the interaction level and ‘‘oscillations’’ can occur at zero distance. With a capability of flavour and charge identifications, we have a chance of using eight appearance and disappearance oscillation channels in the physics study. We have chosen the advanced neutrino detector using the Gd-doped Water Cherenkov technology and studied neutrino oscillations confronting with CC-NSIs at the MOMENT experiment.

Since MOMENT is a medium baseline experiment, the matter effects are relatively small. We have checked the numerical results of oscillation probabilities in vacuum and matter, and found negligible difference with/without matter effects. In order to understand the relevant behavior from NSIs, we have perturbatively derived oscillation probabilities including CC-NSIs at a short and far distance, and tried to analyze parameter correlations of standard neutrino mixing parameters with NSI parameters. We have investigated impacts of the charged current NSIs at neutrino oscillation probabilities, selected the following dominating CC-NSI parameters $\epsilon_{ee}^{s/d}$, $\epsilon_{\mu\mu}^{s/d}$, $\epsilon_{\mu e}^{s/d}$ and $\epsilon_{e\mu}^{s/d}$ for the near detector, and concentrated on ϵ_{ee}^s , $\epsilon_{\mu\mu}^s$, $\epsilon_{\mu\tau}^s$, $\epsilon_{\mu e}^s$, $\epsilon_{\mu e}^d$, $\epsilon_{\tau e}^d$, $\epsilon_{e\mu}^s$, $\epsilon_{e\tau}^s$ and $\epsilon_{e\mu}^d$ for the far detector.

A near detector at MOMENT is good at detecting the zero-distance effects induced by NSIs while the oscillation pattern would have not been developed in the standard neutrino oscillation paradigm. With near and far detectors, we have found that CC-NSIs can induce bias in precision measurements of standard mixing parameters. Taking δ_{cp} and θ_{23} as an example, we have found degeneracies after introducing CC-NSI parameters. With a non-maximal θ_{23} , its degeneracy with the standard CP phase δ_{CP} gets much worse if CC-NSIs appear at the neutrino production and detection processes. The current bounds on NSI parameters governing the neutrino productions and detections are about one order of magnitude stronger than those related to neutrino propagation in matter. Our study has shown that a combination of near and far detectors at MOMENT is able to provide lower bounds on CC-NSIs where a factor of a few can be envisaged. We have found strong correlations of NSIs and constrained NSI parameters using a combination of near and far detectors at MOMENT. Compared with the current experimental bounds, MOMENT can set the lower bound for most of the related NSI parameters by almost a factor of two, as shown in Table III.

However, the feasibility of physics performance at MOMENT strongly depends on the research and development of the accelerator facility and the advanced neutrino detection technology. In the future, results will be further improved by tuning the beam energy and optimizing the baseline. We hope that our study will boost the R&D activities for MOMENT.

VI. ACKNOWLEDGEMENT

This work is supported by the start-up funding from SYSU and the National Natural Science Foundation of China under Grant No. 11505301. YBZ appreciates valuable discussions with Steven Wong and Amir Khan. We would like to thank the accelerator working group of MOMENT for fruitful discussions concerned with neutrino fluxes. Furthermore, we are grateful to IHEP colleagues for collaborations, especially Jingyu Tang, Yu-Feng Li, Miao He and Nikos Vassilopoulos.

-
- [1] B. Aharmim et al. Combined Analysis of all Three Phases of Solar Neutrino Data from the Sudbury Neutrino Observatory. *Phys. Rev.*, C88:025501, 2013.
 - [2] R. Wendell et al. Atmospheric neutrino oscillation analysis with sub-leading effects in Super-Kamiokande I, II, and III. *Phys. Rev.*, D81:092004, 2010.
 - [3] S. Abe et al. Precision Measurement of Neutrino Oscillation Parameters with KamLAND. *Phys. Rev. Lett.*, 100:221803, 2008.
 - [4] K. Abe et al. Precise Measurement of the Neutrino Mixing Parameter θ_{23} from Muon Neutrino Disappearance in an Off-Axis Beam. *Phys. Rev. Lett.*, 112(18):181801, 2014.
 - [5] P. Adamson et al. First measurement of muon-neutrino disappearance in NOvA. *Phys. Rev.*, D93(5):051104, 2016.
 - [6] Y. Abe et al. Improved measurements of the neutrino mixing angle θ_{13} with the Double Chooz detector. *JHEP*, 10:086, 2014. [Erratum: *JHEP*02,074(2015)].
 - [7] Feng Peng An et al. Measurement of electron antineutrino oscillation based on 1230 days of operation of the Daya Bay experiment. *Phys. Rev.*, D95(7):072006, 2017.
 - [8] J. H. Choi et al. Observation of Energy and Baseline Dependent Reactor Antineutrino Disappearance in the RENO Experiment. *Phys. Rev. Lett.*, 116(21):211801, 2016.
 - [9] G. L. Fogli, E. Lisi, A. Marrone, D. Montanino, A. Palazzo, and A. M. Rotunno. Global analysis of neutrino masses, mixings and phases: entering the era of leptonic CP violation searches. *Phys. Rev.*, D86:013012, 2012.
 - [10] D. V. Forero, M. Tortola, and J. W. F. Valle. Neutrino oscillations refitted. *Phys. Rev.*, D90(9):093006, 2014.
 - [11] M. C. Gonzalez-Garcia, Michele Maltoni, and Thomas Schwetz. Updated fit to three neutrino mixing: status of leptonic CP violation. *JHEP*, 11:052, 2014.
 - [12] Ivan Esteban, M. C. Gonzalez-Garcia, Michele Maltoni, Ivan Martinez-Soler, and Thomas Schwetz. Updated fit to three neutrino mixing: exploring the accelerator-reactor complementarity. *JHEP*, 01:087, 2017.
 - [13] V. Barger, D. Marfatia, and K. Whisnant. Off-axis beams and detector clusters: Resolving neutrino parameter degeneracies. *Phys. Rev.*, D66:053007, 2002.
 - [14] Hisakazu Minakata, Hiroshi Nunokawa, and Stephen J. Parke. Parameter degeneracies in neutrino oscillation measurement of leptonic CP and T violation. *Phys. Rev.*, D66:093012, 2002.
 - [15] K. Abe et al. Measurements of neutrino oscillation in appearance and disappearance channels by the T2K experiment with 6.6×10^{20} protons on target. *Phys. Rev.*, D91(7):072010, 2015.
 - [16] P. Adamson et al. First measurement of electron neutrino appearance in NOvA. *Phys. Rev. Lett.*, 116(15):151806, 2016.
 - [17] R. Acciarri et al. Long-Baseline Neutrino Facility (LBNF) and Deep Underground Neutrino Experiment (DUNE). 2015.
 - [18] K. Abe et al. A Long Baseline Neutrino Oscillation Experiment Using J-PARC Neutrino Beam and Hyper-Kamiokande. 2014.
 - [19] Fengpeng An et al. Neutrino Physics with JUNO. *J. Phys.*, G43(3):030401, 2016.
 - [20] Soo-Bong Kim. New results from RENO and prospects with RENO-50. *Nucl. Part. Phys. Proc.*, 265-266:93–98, 2015.
 - [21] Shakeel Ahmed et al. Physics Potential of the ICAL detector at the India-based Neutrino Observatory (INO). *Pramana*, 88(5):79, 2017.
 - [22] M. G. Aartsen et al. Letter of Intent: The Precision IceCube Next Generation Upgrade (PINGU). 2014.
 - [23] S. Adrian-Martinez et al. Letter of intent for KM3NeT 2.0. *J. Phys.*, G43(8):084001, 2016.
 - [24] M. C. Gonzalez-Garcia, M. M. Guzzo, P. I. Krastev, H. Nunokawa, O. L. G. Peres, V. Pleitez, J. W. F. Valle, and R. Zukanovich Funchal. Atmospheric neutrino observations and flavor changing interactions. *Phys. Rev. Lett.*, 82:3202–3205, 1999.
 - [25] Sven Bergmann. The Solar neutrino problem in the presence of flavor changing neutrino interactions. *Nucl. Phys.*, B515:363–383, 1998.
 - [26] Sven Bergmann and Alex Kagan. Z - induced FCNCs and their effects on neutrino oscillations. *Nucl. Phys.*, B538:368–386, 1999.
 - [27] S. Bergmann, M. M. Guzzo, P. C. de Holanda, P. I. Krastev, and H. Nunokawa. Status of the solution to the solar neutrino problem based on nonstandard neutrino interactions. *Phys. Rev.*, D62:073001, 2000.
 - [28] Sven Bergmann, H. V. Klapdor-Kleingrothaus, and Heinrich Pas. Lepton number violation interactions and their effects on neutrino oscillation experiments. *Phys. Rev.*, D62:113002, 2000.
 - [29] A. M. Gago, M. M. Guzzo, H. Nunokawa, W. J. C. Teves, and R. Zukanovich Funchal. Probing flavor changing neutrino interactions using neutrino beams from a muon storage ring. *Phys. Rev.*, D64:073003, 2001.

- [30] A. M. Gago, M. M. Guzzo, P. C. de Holanda, H. Nunokawa, O. L. G. Peres, V. Pleitez, and R. Zukanovich Funchal. Global analysis of the postSNO solar neutrino data for standard and nonstandard oscillation mechanisms. *Phys. Rev.*, D65:073012, 2002.
- [31] M. M. Guzzo, P. C. de Holanda, and O. L. G. Peres. Effects of nonstandard neutrino interactions on MSW - LMA solution to the solar neutrino problems. *Phys. Lett.*, B591:1–6, 2004.
- [32] Arman Esmaili and Alexei Yu. Smirnov. Probing Non-Standard Interaction of Neutrinos with IceCube and DeepCore. *JHEP*, 06:026, 2013.
- [33] Yu-Feng Li and Ye-Ling Zhou. Shifts of neutrino oscillation parameters in reactor antineutrino experiments with non-standard interactions. *Nucl. Phys.*, B888:137–153, 2014.
- [34] Jiajun Liao, Danny Marfatia, and Kerry Whisnant. Degeneracies in long-baseline neutrino experiments from nonstandard interactions. *Phys. Rev.*, D93(9):093016, 2016.
- [35] Jiajun Liao and Danny Marfatia. Impact of nonstandard interactions on sterile neutrino searches at IceCube. *Phys. Rev. Lett.*, 117(7):071802, 2016.
- [36] Jiajun Liao, Danny Marfatia, and Kerry Whisnant. Nonmaximal neutrino mixing at $\text{NO}\nu\text{A}$ from nonstandard interactions. *Phys. Lett.*, B767:350–353, 2017.
- [37] Jordi Salvado, Olga Mena, Sergio Palomares-Ruiz, and Nuria Rius. Non-standard interactions with high-energy atmospheric neutrinos at IceCube. *JHEP*, 01:141, 2017.
- [38] Jiajun Liao, Danny Marfatia, and Kerry Whisnant. Nonstandard neutrino interactions at DUNE, T2HK and T2HKK. *JHEP*, 01:071, 2017.
- [39] Pilar Coloma, Peter B. Denton, M. C. Gonzalez-Garcia, Michele Maltoni, and Thomas Schwetz. Curtailing the Dark Side in Non-Standard Neutrino Interactions. *JHEP*, 04:116, 2017.
- [40] Alakabha Datta, Jiajun Liao, and Danny Marfatia. A light Z' for the R_K puzzle and nonstandard neutrino interactions. *Phys. Lett.*, B768:265–269, 2017.
- [41] Jiajun Liao, Danny Marfatia, and Kerry Whisnant. Nonstandard interactions in solar neutrino oscillations with Hyper-Kamiokande and JUNO. 2017.
- [42] Tommy Ohlsson. Status of non-standard neutrino interactions. *Rept. Prog. Phys.*, 76:044201, 2013.
- [43] O. G. Miranda and H. Nunokawa. Non standard neutrino interactions: current status and future prospects. *New J. Phys.*, 17(9):095002, 2015.
- [44] Jun Cao et al. Muon-decay medium-baseline neutrino beam facility. *Phys. Rev. ST Accel. Beams*, 17:090101, 2014.
- [45] Mattias Blennow, Pilar Coloma, and Enrique Fernandez-Martinez. The MOMENT to search for CP violation. *JHEP*, 03:197, 2016.
- [46] Carla Biggio, Mattias Blennow, and Enrique Fernandez-Martinez. General bounds on non-standard neutrino interactions. *JHEP*, 08:090, 2009.
- [47] Joachim Kopp, Manfred Lindner, Toshihiko Ota, and Joe Sato. Non-standard neutrino interactions in reactor and super-beam experiments. *Phys. Rev.*, D77:013007, 2008.
- [48] Pouya Bakhti and Yasaman Farzan. CP-Violation and Non-Standard Interactions at the MOMENT. *JHEP*, 07:109, 2016.
- [49] Nikos Vassilopoulos. Private communications.
- [50] Jean-Eric Campagne, M. Maltoni, M. Mezzetto, and T. Schwetz. Physics potential of the CERN-MEMPHYS neutrino oscillation project. *JHEP*, 04:003, 2007.
- [51] L. Agostino, M. Buizza-Avanzini, M. Dracos, D. Duchesneau, M. Marafini, M. Mezzetto, L. Mosca, T. Patzak, A. Tonazzo, and N. Vassilopoulos. Study of the performance of a large scale water-Cherenkov detector (MEMPHYS). *JCAP*, 1301:024, 2013.
- [52] Patrick Huber and Thomas Schwetz. A Low energy neutrino factory with non-magnetic detectors. *Phys. Lett.*, B669:294–300, 2008.
- [53] Y. Itow et al. The JHF-Kamioka neutrino project. In *Neutrino oscillations and their origin. Proceedings, 3rd International Workshop, NOON 2001, Kashiwa, Tokyo, Japan, December 508, 2001*, pages 239–248, 2001.
- [54] Enrique Fernandez-Martinez. The $\gamma = 100$ beta-Beam revisited. *Nucl. Phys.*, B833:96–107, 2010.
- [55] Mauro Mezzetto. Physics potential of the $\gamma=100,100$ beta beam. *Nucl. Phys. Proc. Suppl.*, 155:214–217, 2006.
- [56] E. A. Paschos and J. Y. Yu. Neutrino interactions in oscillation experiments. *Phys. Rev.*, D65:033002, 2002.
- [57] Patrick Huber, M. Lindner, and W. Winter. Simulation of long-baseline neutrino oscillation experiments with GLoBES (General Long Baseline Experiment Simulator). *Comput. Phys. Commun.*, 167:195, 2005.
- [58] Patrick Huber, Joachim Kopp, Manfred Lindner, Mark Rolinec, and Walter Winter. New features in the simulation of neutrino oscillation experiments with GLoBES 3.0: General Long Baseline Experiment Simulator. *Comput. Phys. Commun.*, 177:432–438, 2007.
- [59] C. Patrignani et al. Review of Particle Physics. *Chin. Phys.*, C40(10):100001, 2016.